Low Temperature CO Sensitive Nanostructured WO_3 Thin Films Doped with Fe

Sensors and Actuators B (Accepted, 2011)

M.Ahsan[1], T.Tesfamichael[1], M. Ionescu[2], J. Bell[1] and N. Motta[1]

[1]School of Engineering Systems, Built Environment and Engineering, Queensland University of Technology, 2 George Street, Brisbane, Queensland 4001, Australia.
[2]Australian Nuclear Science and Technology Organization, New Illawara Road, Lucas Heights, NSW 2232, Australia.

Corresponding Author: Mohammed Ahsan, School of Engineering Systems, Faculty of BEE, 2 George Street, Brisbane, Queensland 4001, Australia, Email: m.ahsan@qut.edu.au, Phone: 0061731384186, Fax: 0061731381522.

Abstract

Nanostructured tungsten oxide thin film based gas sensors have been developed by thermal evaporation method to detect CO at low operating temperatures. The influence of Fe-doping and annealing heat treatment on microstructural and gas sensing properties of these films have been investigated. Fe was incorporated in WO_3 film by co-evaporation and annealing was performed at 400^{o}C for 2 hours in air. AFM analysis revealed a grain size of about 10-15 nm in all the films. GIXRD analysis showed that as-deposited films are amorphous and annealing at 400^{o}C improved the crystallinity. Raman and XRD analysis indicated that Fe is incorporated in the WO_3 matrix as a substitutional impurity, resulting in shorter O-W-O bonds and lattice cell parameters. Doping with Fe contributed significantly towards CO sensing performance of WO_3 thin films. A good response to various concentrations (10-1000 ppm) of CO has been achieved with 400^{o}C annealed Fe-doped WO_3 film at a low operating temperature of 150^{o}C.

Keywords

Tungsten oxide, nanostructured thin films, gas sensing, doping, thermal evaporation, CO sensor.

1. Introduction

Tungsten oxide (WO_3) is an n-type wide band gap metal oxide semiconductor. Like other metal oxides such as SnO_2, TiO_2, In_2O_3 and ZnO, WO_3 has become a promising material for gas sensing devices due to its inherent electrical conductivity and excellent sensitivity and selectivity towards various gases such as NO_2 [1], NH_3 [2], H_2S [3], O_3 [4], H_2 [5] and Volatile Organic Compounds (VOC) [6]. However, as for any other metal oxide based gas

sensor, they operate efficiently only in the temperature range 200^{o}C-500^{o}C [7]. Low fabrication costs combined with low power consumption and a promise of high gas sensitivity towards specific gases are the driving force behind research on WO_3 for improved gas sensing properties. Deposition techniques of WO_3 films vary from acidic precipitation [8], RF sputtering [9], magnetron sputtering [10, 11], hard template route [12], pulsed laser deposition [13], solgel [6] and thermal evaporation [14, 15]. The gas sensing mechanism is based on bulk resistance changes of the WO_3 film induced by reactions between the target gases and the film surface. In air environment, oxygen molecules adsorb onto the surface of metal oxide layer to form O_2^-, O^- and O^{2-} species by extracting electrons from the conduction band depending on the temperature [16] and type of metal oxide (n-type or p-type). For n-type sensor material like WO_3 and a reducing gas, the gas reacts with oxygen ions to form neutral molecules, leading to electron transfer to the sensor material and a resulting decrease in resistance. The microstructural properties of the film have a significant impact on sensing performance. The grain size, film thickness, porosity and heat treatment control the sensor performance. Film thickness can have significant effect in optimizing sensor selectivity and sensitivity [17]. Nanosized materials have a very large surface area which offers more surface/gas interaction thereby enhancing the sensing properties. Sensing measurements on nanostructured WO_3 deposited by thermal evaporation have shown promising performances towards sub-ppm concentrations of NO_2 [14]. Mesoporous nanostructured WO_3 films have shown a high sensitivity to NO_2 even at low concentrations [12]. WO_3 thin films with smaller grain size obtained by rf sputtering have shown enhanced sensitivity to oxidizing gases [18]. Annealing of WO_3 films after deposition has been reported to improve crystallinity and well defined grain boundaries in the film [11, 19, 20]. The addition of metals or metal oxides to WO_3 film can also enhance the sensor performance. Tungsten oxide co-loaded with TiO_2 shows an enhanced sensing performance to NO and NO_2 [21]. Microstructural analysis of co-evaporated films of TiO_2 and WO_3 powders revealed nanoporous films with enhanced porosity [15]. The sensing performance for NO_2, O_3 and C_2H_5OH is also enhanced by using mixed tungsten and iron oxide thin films [9]. Addition of La_2O_3 to WO_3 nanoparticles improved the response towards VOC and the highest gas response shifted towards low temperature [6]. Improved response towards NO_2 by introducing Cu as a catalytic additive in WO_3 films has also been reported. This was mainly attributed to copper segregating at the material surface as Cu(I) [12]. However, there is little evidence indicating response of WO_3 thin films towards CO in the literature [22].

Inclusion of noble metal impurities such as Au, Ag, Pd or metal oxides such as TiO_2 in WO_3 thin films have shown an improved sensitivity towards various gases, which is mainly attributed to the noble metal catalytic effect on the gas/surface interaction [23, 24]. However, gas sensing properties of iron-doped WO_3 thin films have not been well documented. In this paper, iron has been used to dope the WO_3 thin films. Since iron has a similar atomic radius (0.64 nm) as W (0.62 nm), it can be introduced as a substitutional impurity in the WO_3 crystal structure to produce crystal distortions, and its influence on physical, chemical, electronic and gas sensing properties can be investigated. Recently, the addition of Fe to electron beam evaporated (EBE) films has been shown to improve sensitivity towards NO_2 and acetaldehyde at 200^{o}C [25, 26]. In this paper, we present the CO sensing performance of iron-doped thermally evaporated WO_3 thin films at a lower operating temperature of 150^{o}C and discuss this from a microstructural point of view.

2. Experimental

2.1 Sample preparation

Thermal evaporation was used to deposit thin films of tungsten oxide and iron-doped tungsten oxide (0.5 at% Fe). WO_3 thin films were deposited on silicon substrates with interdigitated Pt electrodes (Electronics Design Center, Case Western Reserve University, Cleveland, USA). The size of the substrate was 8 mm x 8 mm x 0.5 mm. The electrode fingers have a line width and height of 100 μm and 300 nm, respectively. Powders of tungsten oxide (99.9% purity, grain size 20 μm) and iron (99.9% purity, grain size 100 μm) from Sigma Aldrich Pty Ltd, were used as evaporation sources. Before the deposition, the powders were placed in dessicator to avoid any moisture and decontamination. For the purpose of doping, iron was mixed thoroughly with WO_3 and the mixture was evaporated. A bell jar type PVD unit (Varian Coater with AVT Control System, Australia) was used to deposit the WO_3 thin films. The substrates were mounted on a substrate holder which was placed at a distance of 38 cm in line of sight from the evaporation source. Deposition was carried out at 4 x 10^{-5} mbar. Powder was deposited onto the substrates at a rate of 35 nm per second. A quartz crystal film thickness monitor was used to control the thickness of films. The film thickness was restricted to 300 nm and the effect of grain size, porosity, crystallinity and heat treatment for a given film thickness has been investigated. After the deposition, the films were annealed at 400^{o}C for 2 hours in air to improve the microstructural properties and relieve any thermal stresses in the films.

2.2 Sample characterization

A JEOL 1200 TEM was used at an accelerating voltage of 120 kV to investigate the size and shape of WO_3 nanoparticles, crystalline structure and distribution of dopant in the film. An NT-MDT P47 Solver Scanning Probe Microscope was used to study the surface morphology of the films. The WO_3 film surface was scanned by a silicon tip (radius of curvature 10 nm) in semi-contact mode over an area ranging from 500 nm^2 to 2000 nm^2. The mean grain size and grain distribution and surface roughness were determined by using the Nova NT-MDT Image Analysis Software. The concentration profile of constituent elements in WO_3 film was determined using RBS analysis. RBS measurements were carried out with a 1.8 MeV He^+ beam under a vacuum of 7 x 10^{-6} mbar. XPS analysis was performed using Kratos AXIS Ultra XPS incorporating a 165 mm hemispherical electron energy analyser, and using monochromatic Al Kα X-rays (1486.6 eV) at 150 W (15 kV, 10 mA), incident at 45^o to the sample surface. Photoelectron data was collected at take off angle of 90^o. Survey (wide) scans were taken at analyser pass energy of 160 eV and multiplex (narrow) high resolution scans at 20 eV. Survey scans were carried out over 1200-0 eV binding energy range with 1.0 eV steps and a dwell time of 100 ms. Narrow high-resolution scans were run with 0.05 eV steps and 250 ms dwell time. Base pressure in the analysis chamber was 1.0 x 10^{-9} mbar and during sample analysis 1.0 x 10^{-8} mbar. Depth profiling of the film was also carried out by etching the surface with Ar source at a rate of 10 nm per second. GIXRD analysis was performed on PANanalytical XPert Pro Multi Purpose Diffractometer (MPD). A Cu K_α radiation of wavelength 1.540 Å was used. The incident angle was kept at 2^o and the 2θ range was kept between 10^o to 85^o with a step size of 0.05^o. Raman measurements were performed using an Oceanoptics QE 6500 spectrometer. A 532 nm line from an argon ion laser was used as the excitation source. To avoid local heating of the samples, small power of about 5 mW was used on the samples. A raman shift between wavenumbers 200 cm^{-1} and 1200 cm^{-1} has been measured. The WO_3 sensor responses to various concentrations (10-1000 ppm) of CO at various operating temperatures (100^{o}C to 300^{o}C) were measured. CO was diluted in synthetic air to achieve the desired concentrations. For all the experiments, the total flow was adjusted to 200 sccm. The response of the films to reducing gases such as CO denoted as $S_{reducing}$ is defined as the ratio:

$$S_{reducing} = \frac{R_{air} - R_{gas}}{R_{gas}} \qquad (1)$$

where R_{air} is the resistance in air under stationary conditions and R_{gas} represents the resistance after the sensor is exposed to the target gas during a definite time. Equation 1 can be applied for n-type material such as WO_3 and reducing gas such as CO.

The response curve was recorded under a continuous flow of known amount of CO. A sequence control computer was utilized to computerize the pulse sequence of the CO concentrations. Initially, synthetic air was passed through the chamber at testing temperature until the stable baseline resistance was observed. Then a sequence of target gas pulse was generated for 10 minutes followed by synthetic air pulse. This procedure was continued until a stable baseline was observed after alternate pulses. This was followed by the experimental sequence of pulses and data was recorded. Each sensor was tested at temperatures between 100°C to 300°C at intervals of 50°C under various concentrations of CO, and optimum operating temperature was determined. This was followed by two full range tests for each sensor and CO at the optimum operating temperature.

3. Results and Discussion

The as-deposited as well as 400°C annealed WO_3 films did not show any response to CO in the temperature range 100°C-300°C. However, after doping with Fe and subsequent annealing, a maximum response towards CO was observed at an operating temperature of 150°C. Figure 1 shows the dynamic resistance curve and response of 400°C annealed Fe-doped WO_3 film upon exposure to CO.

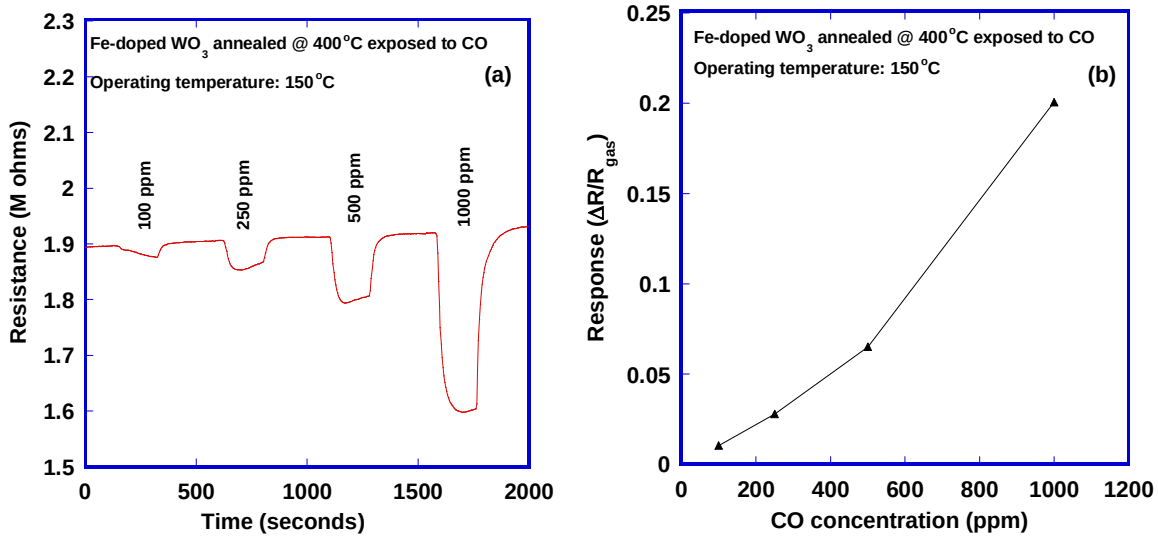

Figure 1: Dynamic resistance curve (a) and response (b) of nanostructured Fe-doped WO_3 films annealed at 400°C for 2 hours in air.

The film shows a stable response curve with a maximum response of S=20% and a small response time of 64s to 1000 ppm CO. The dominant species on the film surface at 150^{o}C is O_2^- [27]. The conduction mechanism is governed by the following equation [28].

$$2CO + O_2^- \rightarrow 2CO_2 + e^- \qquad (2)$$

Upon exposure to CO, carbon dioxide is formed with the consequent injection of free charge carriers into the conduction band. This causes a drop in film resistance.
The doping effect of metal additives on gas sensors is usually attributed to the catalytic effects of dopants favouring oxygen transfer from chemical aspect and/or electron transfer from electronic aspect [29]. In this study, we consider the doping effect of Fe from a morphological and crystal structure point of view.

Table 1: Grain size of WO_3 and Fe-doped WO_3 films before and after annealing at 400^{o}C for 2 hours in air.

Film	**as-deposited WO_3**	**as-deposited Fe-doped WO_3**	**WO_3 annealed at 400^{o}C**	**Fe-doped WO_3 annealed at 400^{o}C**
Grain size	13 nm	15 nm	5 nm	10 nm

Table 1 shows the grain size information of the films before and after annealing at 400^{o}C for 2 hours in air, obtained by AFM image analysis software for AFM images and visual examination for TEM images. The surface topography of as-deposited WO_3 film (Figure 2a) shows a nanostructured surface with well defined grains of mean size 13 nm and surface roughness of 0.5 nm respectively. The surface of as-deposited Fe-doped WO_3 film (Figure 2b) also reveals well defined grain boundaries with an average grain size of 15 nm. However, the grains appear to be densely packed compared to pure WO_3 film (Figure 2a). Addition of iron also resulted in an increase in roughness to 0.6 nm compared to 0.5 nm for as-deposited WO_3 film.

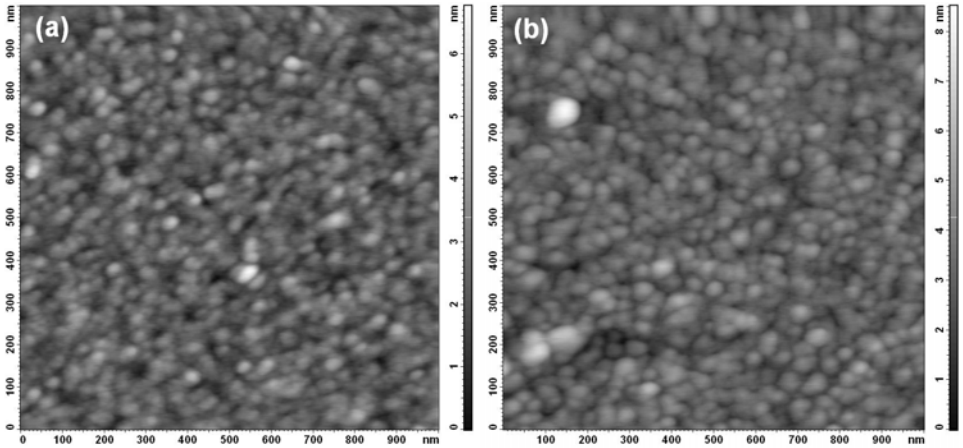

Figure 2: AFM semicontact mode images of as-deposited (a) WO_3 and (b) Fe-doped WO_3 film.

Annealing of WO_3 films at 400^{o}C in air for 2 hours resulted in a mean grain size of ~ 5 nm (Figure 3a). Porosity is also evident after annealing at 400^{o}C. In the case of Fe-doped WO_3 film, annealing at 400^{o}C reveals a mean grain size of the order of 10 nm (Figure 3b). It can be observed that after annealing at 400^{o}C, both the films have smaller grain size. The high deposition rate during evaporation resulted in highly amorphous films made up of clusters (particles). The nucleation, successive grain growth and coalescence during annealing at 400^{o}C transformed these clusters into smaller grains.

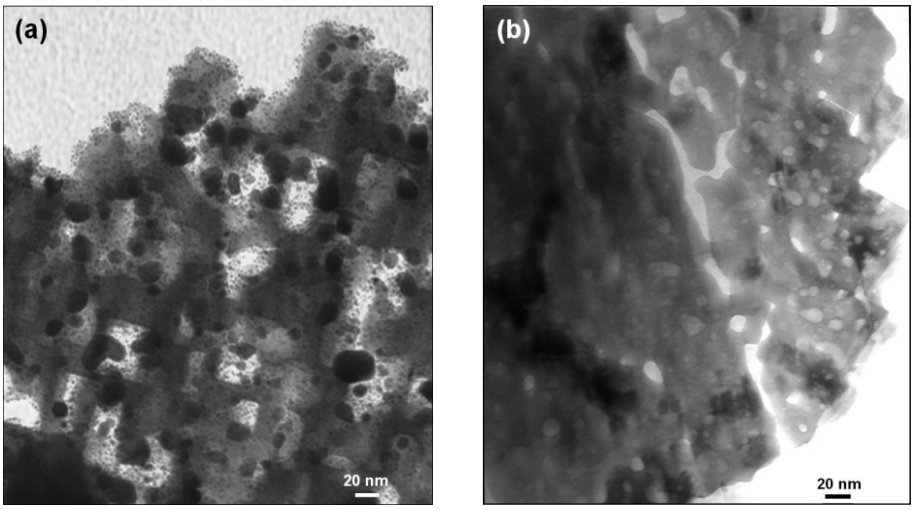

Figure 3: TEM images of (a) WO_3 and (b) Fe-doped WO_3 films annealed at 400^{o}C for 2 hours in air.

Figure 4 shows the RBS spectra of as-deposited WO_3 and Fe-doped WO_3 films. The spectra exhibit a typical staircase structure with each step associated with an element in the sample. Well separated and high intensity of W peak from the film is due to the higher mass (atomic weight) of W compared to O or other trace elements such as N. Also the He particles are

scattered with much higher recoil energy in the film than from the substrate (Si) in this elastic scattering process.

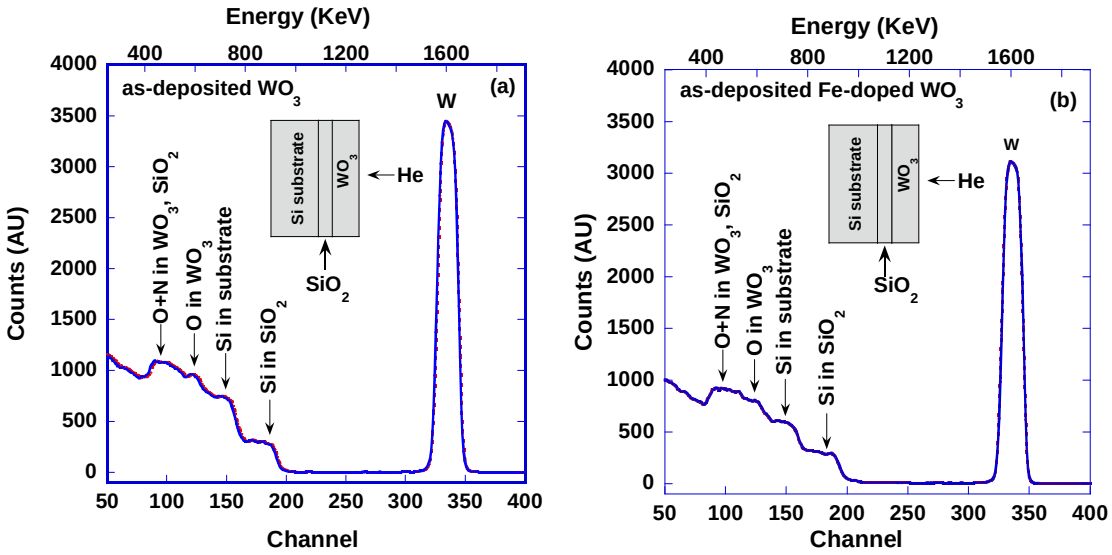

Figure 4: RBS spectra of as-deposited (a) WO_3 and (b) Fe-doped WO_3 thin films.

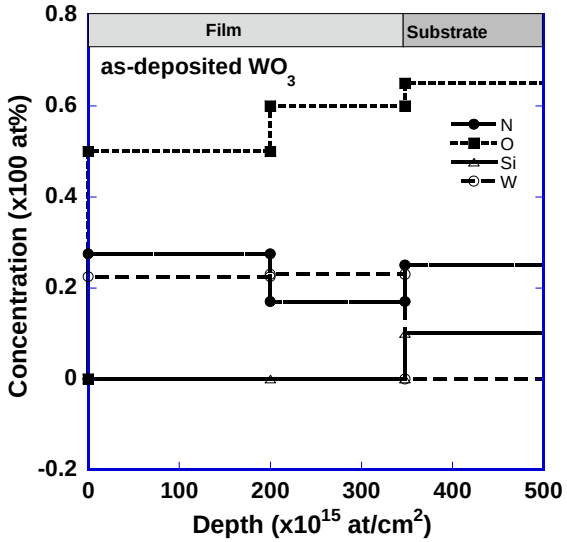

Figure 5: RBS depth profile of as-deposited WO_3 thin films.

The depth profile of WO_3 film (Figure 5) indicates the presence of O, N and W. RBS is limited by resolution for light elements such as B, C, O, N and poor resolution of elements with similar masses. The presence of oxygen can be attributed to adsorbed oxygen from the environment in addition to the lattice oxygen within the film. The depth profile of as-deposited Fe-doped WO_3 film shows O, W, N and Fe (Figure 6a). From RBS analysis, the total amount of Fe in the film was found to be only about 0.5 at%. The low concentration of Fe (0.5 at%) is shown in the enlarged Y-axis figure (Figure 6b). AFM results have shown that addition of Fe resulted in slight increase in grain size to 15 nm. Addition of Fe appears to have slightly changed the stoichiometry of the film (change in amount of O and W).

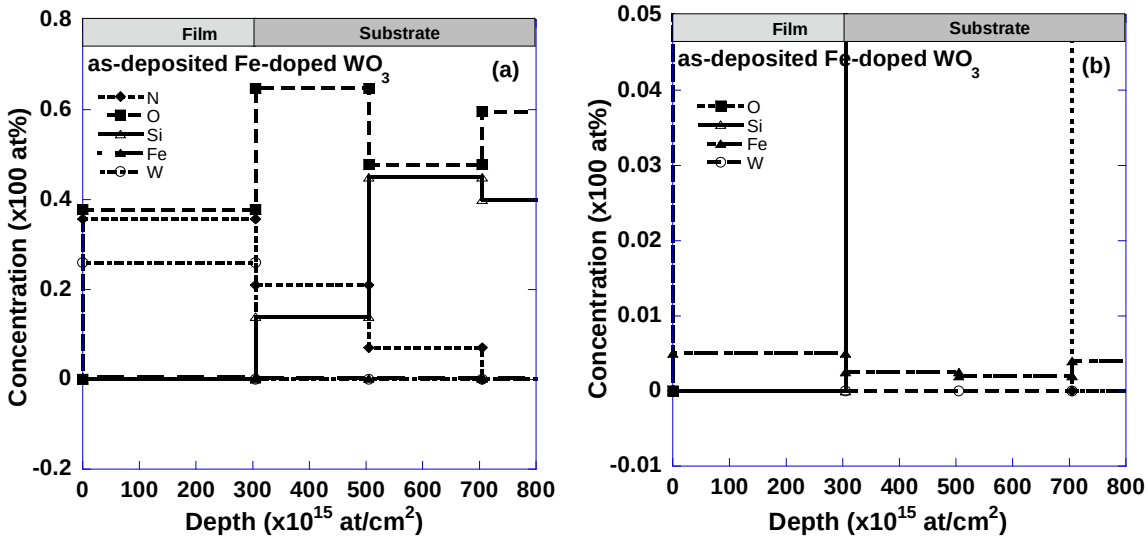

Figure 6: RBS depth profile of as-deposited Fe-doped WO_3 thin films.

Figure 7 shows the GIXRD patterns of as-deposited and annealed WO_3 and Fe-doped WO_3 films. The as-deposited films did not show any diffraction pattern, indicating that these films are highly amorphous. However, after annealing at 400^{o}C, significant crystallinity is observed in both the films, indicated by appearance of diffraction peaks in GIXRD pattern. For the 400^{o}C annealed WO_3 film, the peaks obtained at $2\theta = 24.112^o$, 28.538^o, 34.361^o, 41.615^o, 49.843^o, 55.684^o, 61.941^o are closely related to monoclinic WO_3 phase [30]. It should be noted that the lattice parameters of orthorhombic WO_3 phase are very similar to monoclinic phase, and thus, these two phases cannot be distinguished within the accuracy of GIXRD data. It has been reported that the two intense peaks observed at $2\theta=24.278^o$ and 34.117^o are associated to (2 0 0) and (2 2 0) monoclinic planes of WO_3 corresponding to $d=3.663^o$ and 2.626 Å, respectively [31]. The lattice parameters were found to be a = 7.375 Å, b = 7.375 Å and c = 3.903 Å and its unit cell volume is about 212.38 Å^3.

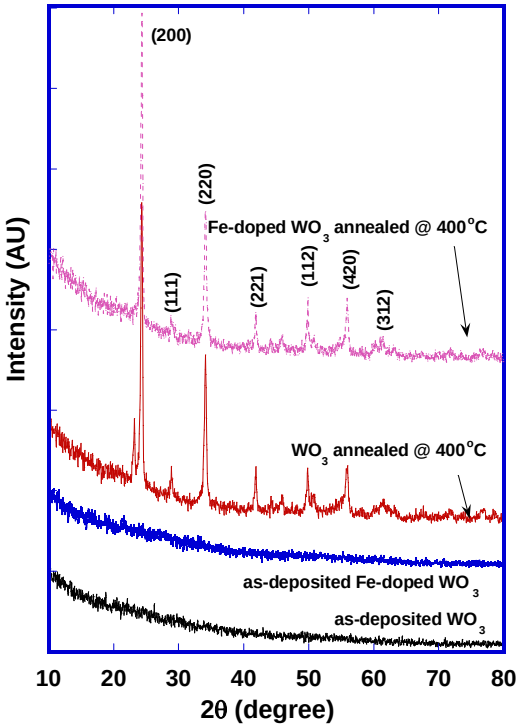

Figure 7: GIXRD spectra of as-deposited and annealed WO_3 and Fe-doped WO_3 films.

In case of 400°C annealed Fe-doped WO_3 film, peaks are observed at $2\theta = 24.322^o$, 28.820^o, 34.082^o, 41.821^o, 49.863^o and 55.866^o. Similar to the 400°C annealed WO_3 film, these peaks are also closely related to monoclinic WO_3 phase [30]. Moreover, the peak positions of both the annealed films match closely. The observed matching of GIXRD pattern of WO_3 and Fe-doped WO_3 film can be explained from a crystallographic viewpoint. The ionic radius of W^{6+} (0.62 Å) is similar to that of Fe^{3+} (0.64 Å). Moreover, the W^{6+} is octahedrally coordinated with O^{2-}. In Iron oxides, the crystal field stabilization energy of Fe^{3+} is higher for octahedral orientation than for tetrahedral orientation [32]. Therefore, Fe^{3+} can fulfil the same coordination as that of W^{6+}. Consequently, Fe-doped WO_3 film shows the same crystal structure as that of WO_3 film. Similar crystal structures were also observed between pure ZnO and Fe-doped ZnO by Han et al [33]. The observed shift in peak positions of annealed Fe-doped WO_3 film compared to annealed WO_3 film, although very little (0.02 Å), can be attributed to the small difference between the ionic radii of W^{6+} and Fe^{3+}. The ionic radius of Fe^{3+} is slightly greater than that of W^{6+} and this can cause slight distortion in the crystal lattice when WO_3 is doped with Fe, and consequently a shift in the diffraction peaks. Such distortions can also produce a number of defects in the film, making it a better candidate for gas sensing.

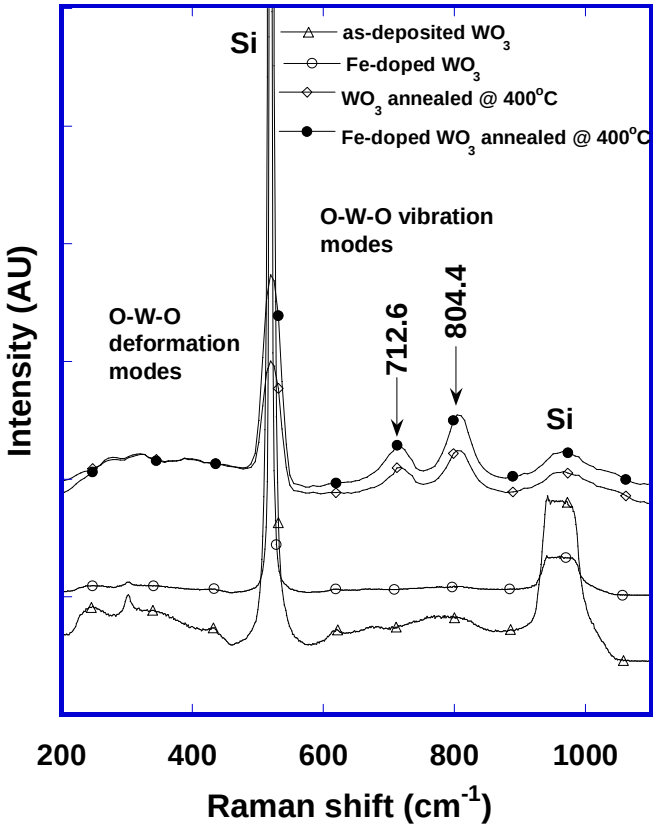

Figure 8: Raman spectra of as-deposited and annealed WO_3 and Fe-doped WO_3 films.

The Raman spectra of as-deposited and 400°C annealed films are shown in Figure 8. Two characteristic Raman bands are associated with WO_3. The first band lies between 200-500 cm^{-1} and is associated with O-W-O bending vibration modes. The second band lies in the range 600-1000 cm^{-1} and is associated with W-O stretching vibration modes. The as-deposited WO_3 and Fe-doped WO_3 films exhibit weak and broad Raman bands centred at 315 cm^{-1}, 799 cm^{-1} and 320 cm^{-1}, 804.4 cm^{-1}, respectively. These features are characteristic of amorphous materials and are usually assigned to O-W-O deformation modes and O-W-O stretching vibration modes of monoclinic WO_3 phase, respectively [13]. This is in accordance with GIXRD observations. Crystallinity of both the WO_3 and Fe-doped WO_3 films increased after annealing at 400°C, as shown by sharp peaks at 707 cm^{-1} and 799 cm^{-1} for WO_3 and at 712.6 cm^{-1} and 804.4 cm^{-1} for Fe-doped WO_3 film which are characteristic of O-W-O stretching vibration modes [34]. Raman results indicate that the annealed films are highly crystalline, which is also supported by GIXRD observations.

Table 2: Comparison of O-W-O stretching vibration mode peak positions of nanostructured WO_3 and Fe-doped WO_3 films annealed at 400°C for 2 hours in air.

	Raman Peak position (cm^{-1})	
WO_3 annealed at 400°C	707	799
Fe-doped WO_3 annealed at 400°C	712.6	804.4
Blue Shift (cm^{-1})	**5.5**	**5.5**

The O-W-O stretching vibration mode peak positions of WO_3 and Fe-doped WO_3 films annealed at 400°C are compared in Table 2. A mean blue shift of about 5.5 cm^{-1} is observed for both the peaks. Such shifts are associated with shortening of O-W-O bonds [35], which corresponds to slightly smaller cell parameters of Fe-doped WO_3 film as compared to WO_3 film. The GIXRD analysis has shown that the lattice parameters of Fe-doped WO_3 film are slightly smaller than WO_3 film. The GIXRD and Raman analysis indicate that addition of Fe to WO_3 film resulted in slight distortion of the lattice structure (shortening of O-W-O bonds), owing to the slightly larger ionic radius of Fe^{3+} over W^{6+}, consequently resulting in a slight shift in XRD as well as Raman peaks. However, the octahedral orientation of WO_3 has been retained after doping with Fe, indicating that the preferred oxidation state of Fe is Fe^{3+}. This is evident from similar XRD patterns of 400°C annealed WO_3 and Fe-doped WO_3 films and no evidence of any Raman peaks associated with Fe in 400°C annealed Fe-doped WO_3 film.

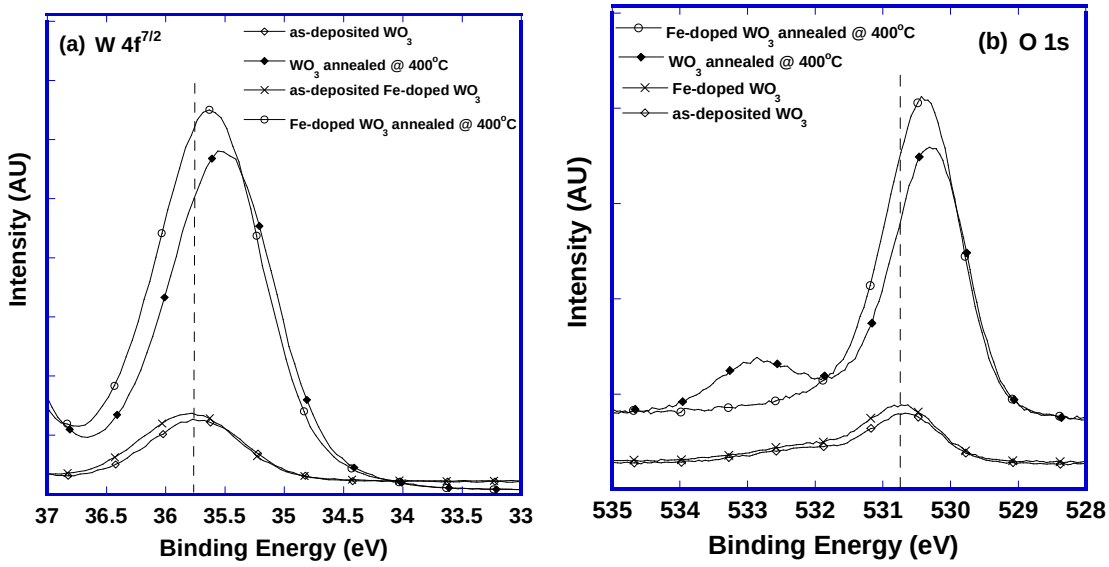

Figure 9: XPS high resolution core level (a) W $4f^{7/2}$ and (b) O 1s spectra of as-deposited and 400°C annealed WO_3 and Fe-doped WO_3 films.

Figure 9 shows the XPS high resolution core level W $4f^{7/2}$ and O 1s spectra of as-deposited and annealed films. For the as-deposited WO_3 film, the core level spectra of W $4f^{7/2}$ is observed at binding energy E_b of 35.74 eV , which corresponds well with the literature reported W $4f^{7/2}$ E_b value of 35.8 eV [36]. The W $4f^{7/2}$ peak shapes becomes sharper after annealing, which indicates that the surface becomes cleaner due to desorption of surface contaminants by annealing. The broadening of the peaks is associated with change in stoichiometry of the sample surface, with the formation of different oxides such as WO_2 or WO [37]. The W $4f^{7/2}$ peak of metallic tungsten is located at 31.50 eV [38]. The W $4f^{7/2}$ peaks located at +4.5, +3 and +1.5 from the metallic tungsten W $4f^{7/2}$ peak are attributed to W^{6+}, W^{5+} and W^{4+} electronic states, respectively [39]. Annealing at 400^{o}C resulted in lowering of W $4f^{7/2}$ binding energy by 0.3 eV, indicating presence of mixed tungsten states [40]. For the as-deposited Fe-doped WO_3 film, the W $4f^{7/2}$ peak is observed at 35.80 eV, closely matching with the literature reported value [41] . The W $4f^{7/2}$ peak in Fe-doped WO_3 film is located at +4.3 eV with respect to the $4f^{7/2}$ peak of metallic tungsten located at 31.5 eV. This indicates formation of mixed W states upon doping with Fe [39]. Compared to pure WO_3 film (W $4f^{7/2}$ peak located at +4.2 eV from metallic tungsten $4f^{7/2}$ peak), doping with Fe appears to have altered the stoichiometry towards nominal WO_3 (+4.3 eV). Annealing this film at 400^{o}C resulted in lowering of W $4f^{7/2}$ binding energy by about 0.2 eV, indicating presence of mixed tungsten states. The downshift of W $4f^{7/2}$ peak is attributed to an increase in number of oxygen vacancies on the surface [42]. It can be explained by the fact that, if an oxygen vacancy exists in the film, the electronic density near its adjacent W atom increases. The 4f level binding energy is expected to be at lower binding energy as the screening of its nucleus is higher because of increased electronic density [42]. Oxygen vacancies play an important role as adsorption sites for gaseous species and eventually, a minor shift of the binding energy may imply greatly enhanced gas sensitivity [43]. XPS analysis has shown that the annealed films have mixed tungsten states, indicating that these films have high number of oxygen vacancies. Changes in band gap values and positions of the valence band maximum and the conduction band minimum have been revealed for different phases of WO_3 due to presence of oxygen vacancies [44]. It has been observed that the energy gap shrinks by about 0.5 eV if an oxygen vacancy is formed [45]. The effect of doping on band gap shifts of WO_3 has also been reported in the literature [45, 46].

The O 1s core level high resolution spectra shows an E_b of 530.7 eV for as-deposited WO_3 film. Annealing at 400^{o}C lowered the binding energy E_b by 0.3 eV, which is same as the downshift observed for W 4f peak after annealing at 400^{o}C. This is most likely a shift of the

Fermi level, corresponding to band bending due to desorption of surface contaminants during annealing at 400^{o}C [11]. A small shoulder centred at about 532.9 eV is observed in the as-deposited film. This shoulder transformed into a peak when the film was annealed at 400^{o}C. Such feature is a characteristic of substoichiometric monoclinic tungsten oxides [47]. The formation and increasing intensity of this feature is in the sequence $WO_3 \rightarrow WO_2$. For the as-deposited Fe-doped WO_3 film, the O 1s binding energy peak is observed at E_b of 530.70 eV, which is same as that observed for as-deposited WO_3 film. Upon annealing this film at 400^{o}C, the binding energy of O 1s lowered by 0.3 eV, which is nearly same in magnitude as that observed for WO_3 film upon annealing at 400^{o}C, attributed to Fermi level shift caused by annealing.

Tungsten oxide commonly operates as gas sensor in the temperature between 200^{o}C-500^{o}C [7] and it is widely accepted that pure WO_3 thin film based gas sensors are not sensitive to carbon monoxide (CO). There is very little evidence of CO sensing performance of pure WO_3 thin films available in literature [22, 48]. In the present study, the as-deposited and annealed WO_3 films did not show any response towards CO. However, after doping with Fe and subsequent annealing at 400^{o}C, the film showed a stable response curve and a good response at a low operating temperature of 150^{o}C. XRD and Raman analysis have revealed that Fe is incorporated in the host WO_3 matrix as a substitutional impurity rather than as a catalyst on the film surface. Fe-doping and subsequent annealing at 400^{o}C has resulted in smaller cell parameters and shortening of O-W-O bonds. XPS analysis revealed that the annealed films contain high number of oxygen vacancies which is highly beneficial for gas sensing. To summarize, the optimum response of Fe-doped WO_3 thin films to CO at a temperature less than 200^{o}C is attributed to a number of factors which include high crystallinity, small grain size, porosity, shortening of O-W-O bonds and oxygen vacancies. The optimum physical, chemical and electrical properties achieved by iron doping and annealing of WO_3 films strongly influenced their response towards CO at a low operating temperature.

4. Conclusions

Nanostructured pure and Fe-doped WO_3 thin films of (300 nm) and grain size of 10-15 nm have been synthesized by thermal evaporation method. The as-deposited films are highly amorphous and annealing at 400^{o}C significantly improved the crystallinity without altering much the grain size. Analysis has shown that Fe was incorporated in WO_3 film as a substitutional impurity in the WO_3 matrix, rather than as a catalyst on the film surface. Fe

incorporation resulted in shortening of lattice cell parameters and O-W-O bonds. The film also contained mixed tungsten states. This has created a number of defects and ultimately high number of oxygen vacancies in the film. By doping with Fe and annealing at 400^{o}C, we have been able to achieve a response to CO at a temperature of 150^{o}C.

Acknowledgements

The authors thank Queensland University of Technology for the support to carry out this research through National and International Research Alliance Program (NIRAP) project. The author deeply acknowledges Australian Institute of Nuclear Science and Engineering for providing support to use RBS facility. The first author is indebted to RMIT University for accessing their gas sensing facility.

References

[1] D.-S. Lee, K.-H. Nam, D.-D. Lee, Effect of substrate on NO_2-sensing properties of WO_3 thin film gas sensors, Thin Solid Films, 375 (2000) 142-146.
[2] T. Mearkawa, J. Tamaki, N. Miura, N. Yamazoe, Gold-loaded tungsten oxide sensor for detection of ammonia in air, Chemistry Letters, (1992) 639-642.
[3] E.P.S. Barrett, G.C. Georgiades, P.A. Sermon, The mechanism of operation of WO_3-based H_2S sensors, Sensors and Actuators B: Chemical, 1 (1990) 116-120.
[4] R. Boulmani, M. Bendahan, C. Lambert-Mauriat, M. Gillet, K. Aguir, Correlation between rf-sputtering parameters and WO_3 sensor response towards ozone, Sensors and Actuators B: Chemical, 125 (2007) 622-627.
[5] M.H. Yaacob, M. Breedon, K. Kalantar-zadeh, W. Wlodarski, Absorption spectral response of nanotextured WO_3 thin films with Pt catalyst towards H_2, Sensors and Actuators B: Chemical, 137 (2009) 115-120.
[6] S. Luo, G. Fu, H. Chen, Z. Liu, Q. Hong, Gas-sensing properties and complex impedance analysis of Ce-added WO_3 nanoparticles to VOC gases, Solid-State Electronics, 51 (2007) 913-919.
[7] P.G. Su, T.T. Pan, Fabrication of a room-temperature NO_2 gas sensor based on WO_3 films and WO_3/MWCNT nanocomposite films by combining polyol process with metal organic decomposition method, Materials Chemistry and Physics, 125 (2011) 351-357.
[8] C. Balázsi, L. Wang, E.O. Zayim, I.M. Szilágyi, K. Sedlacková, J. Pfeifer, A.L. Tóth, P.-I. Gouma, Nanosize hexagonal tungsten oxide for gas sensing applications, Journal of the European Ceramic Society, 28 (2008) 913-917.
[9] E. Comini, L. Pandolfi, S. Kaciulis, G. Faglia, G. Sberveglieri, Correlation between atomic composition and gas sensing properties in tungsten-iron oxide thin films, Sensors and Actuators B: Chemical, 127 (2007) 22-28.
[10] H.-H. Lu, Effects of oxygen contents on the electrochromic properties of tungsten oxide films prepared by reactive magnetron sputtering, Journal of Alloys and Compounds, 465 (2008) 429-435.
[11] T.G.G. Maffeis, D. Yung, L. LePennec, M.W. Penny, R.J. Cobley, E. Comini, G. Sberveglieri, S.P. Wilks, STM and XPS characterisation of vacuum annealed nanocrystalline WO_3 films, Surface Science, 601 (2007) 4953-4957.

[12] E. Rossinyol, A. Prim, E. Pellicer, J. Rodríguez, F. Peiró, A. Cornet, J.R. Morante, B. Tian, T. Bo, D. Zhao, Mesostructured pure and copper-catalyzed tungsten oxide for NO_2 detection, Sensors and Actuators B: Chemical, 126 (2007) 18-23.
[13] K.J. Lethy, D. Beena, R.V. Kumar, V.P.M. Pillai, V. Ganesan, V. Sathe, Structural, optical and morphological studies on laser ablated nanostructured WO_3 thin films, Applied surface Science, 254 (2008) 2369-2376.
[14] A. Ponzoni, E. Comini, M. Ferroni, G. Sberveglieri, Nanostructured WO_3 deposited by modified thermal evaporation for gas-sensing applications, Thin Solid Films, 490 (2005) 81-85.
[15] T. Tesfamichael, N. Motta, T. Bostrom, J.M. Bell, Development of porous metal oxide thin films by co-evaporation, Applied Surface Science, 253 (2007) 4853-4859.
[16] P. Esser, W. Göpel, "Physical" adsorption on single crystal zinc oxide, Surface Science, 97 (1980) 309-318.
[17] G.G. Mandayo, E. Castano, F.J. Gracia, A. Cirera, A. Cornet, J.R. Morante, Strategies to enhance the carbon monoxide sensitivity of tin oxide thin films, Sensors and Actuators B: Chemical, 95 (2003) 90-96.
[18] S. Vallejos, V. Khatko, J. Calderer, I. Gracia, C. Cané, E. Llobet, X. Correig, Micro-machined WO_3-based sensors selective to oxidizing gases, Sensors and Actuators B: Chemical, 132 (2008) 209-215.
[19] D. Meng, T. Yamazaki, Y. Shen, Z. Liu, T. Kikuta, Preparation of WO_3 nanoparticles and application to NO_2 sensor, Applied Surface Science, 256 (2009) 1050-1053.
[20] G. Xie, J. Yu, X. Chen, Y. Jiang, Gas sensing characteristics of WO_3 vacuum deposited thin films, Sensors and Actuators B: Chemical, 123 (2007) 909-914.
[21] K.-i. Shimizu, K. Kashiwagi, H. Nishiyama, S. Kakimoto, S. Sugaya, H. Yokoi, A. Satsuma, Impedancemetric gas sensor based on Pt and WO_3 co-loaded TiO_2 and ZrO_2 as total NO_x sensing materials, Sensors and Actuators B: Chemical, 130 (2008) 707-712.
[22] R.J. Wu, W.C. Chang, K.M. Tsai, J.G. Wu, The Novel CO sensing material CoOOH-WO_3 with Au and SWCNT performance enhancement, Sensors and Actuators B: Chemical, 138 (2009) 35-41.
[23] D.-S. Lee, S.-D. Han, J.-S. Huh, D.-D. Lee, Nitrogen oxides-sensing characteristics of WO_3-based nanocrystalline thick film gas sensor, Sensors and Actuators B: Chemical, 60 (1999) 57-63.
[24] M. Stankova, X. Vilanova, J. Calderer, E. Llobet, J. Brezmes, I. Gràcia, C. Cané, X. Correig, Sensitivity and selectivity improvement of rf sputtered WO_3 microhotplate gas sensors, Sensors and Actuators B: Chemical, 113 (2006) 241-248.
[25] M. Ahsan, T. Tesfamichael, A. Ponzoni, G. Faglia, Sensing Properties of E-Beam Evaporated Nanostructured Pure and Iron-Doped Tungsten Oxide Thin Films, Sensor Letters, 9 (2011) 759-762.
[26] T. Tesfamichael, M. Arita, T. Bostrom, J. Bell, Thin film deposition and characterization of pure and iron-doped electron-beam evaporated tungsten oxide for gas sensors, Thin Solid Films, 518 (2010) 4791-4797.
[27] N. Barsan, M. Schweizer-Berberich, W. Göpel†, Fundamental and practical aspects in the design of nanoscaled SnO_2 gas sensors: a status report, Fresenius' Journal of Analytical Chemistry, 365 (1999) 287-304.
[28] G. Lu, L.E. Ocala, J. Chen, Room-temperature gas sensing based on electron transfer between discrete tin oxide nanocrystals and mutliwalled carbon nanotubes, Advanced Materials, 21 (2009) 2487-2491.
[29] Y. Shimizu, M. Egashira, Basic aspects and challenges of semiconductor gas sensors, in: MRS Bulletin, 1999, pp. 18-24.

[30] J. Diaz-Reyes, F.-M. J.E., J.M. Gutierrez-Arias, M.M. Morin-Castillo, H. Azucena-Coyotecatl, M. Galvan, P. Rodriguez-Fragoso, A. Mendez-Lopez, Optical and structural properties of WO_3 as a function of the annealing temperature, in: O. Frazao (Ed.) 3rd WSEAS International Conference on Sensors and Signals (SENSIG'10), WSEAS Press, Portugal, 2010, pp. 99-104.
[31] S.C. Moulzolf, L.J. LeGore, R.J. Lad, Heteroepitaxial growth of tungsten oxide films on sapphire for chemical gas sensors, Thin Solid Films, 400 (2001) 56-63.
[32] R.M. Cornell, U. Schwertmann, The iron oxides: Structure, properties, reactions, occurences and uses, 2nd ed., Wiley-VCH, Verlag GmbH & Co, 2003.
[33] N. Han, L. Chai, Q. Wang, Y. Tian, P. Deng, Y. Chen, Evaluating the doping effect of Fe, Ti and Sn on gas sensing property of ZnO, Sensors and Actuators B: Chemical, 147 525-530.
[34] E. Salje, K. Viswanathan, Physical properties and phase transitions in WO_3, Acta Crystallographica A, 31 (1975) 356-359.
[35] C. Guery, C. Choquet, F. Dujeancourt, J.M. Tarascon, J.C. LassÃ¨gues, Infrared and X-ray studies of hydrogen intercalation in different tungsten trioxides and tungsten trioxide hydrates, Journal of Solid State Electrochemistry, 1 (1997) 199-207.
[36] J.F. Morar, F.J. Himpsel, G. Hughes, J.L. Jordan, F.R. McFeely, G. Hollinger, High resolution photoemission investigation: The oxidation of W, Journal of Vacuum Science and Technology A: Vacuum, Surfaces and Films, 3 (1985) 1477-1480.
[37] T.G.G. Maffeis, M.W. Penny, R.J. Cobley, E. Comini, G. Sberveglieri, S.P. Wilks, XPS characterization of vacuum annealed nanocrystalline WO_3 films, e-Journal of Surface Science and Nanotechnology, 7 (2009) 319-322.
[38] M. Regragui, M. Addou, A. Outzourhit, J.C. Bernéde, E. El Idrissi, E. Benseddik, A. Kachouane, Preparation and characterization of pyrolytic spray deposited electrochromic tungsten trioxide films, Thin Solid Films, 358 (2000) 40-45.
[39] G. Hollinger, in, Thesis, Universite Claude Bernad, Lyon, 1976.
[40] S. Santucci, C. Cantalini, M. Crivellari, L. Lozzi, L. Ottaiano, M. Passacantando, X-ray photoemission spectroscopy and scanning tunneling spectroscopy study on thermal stability of WO_3 thin films, Journal of Vacuum Science and Technology, 18 (2000) 1077.
[41] J.N. Yao, P. Chen, A. Fujishima, Electrochromic behavior of electrodeposited tungsten oxide thin films, Journal of Electroanalytical Chemistry, 406 (1996) 223-226.
[42] C.G. Granqvist, CRC Handbook of Solid State Electrochemistry, CRC Press, Inc., Cleveland and Ohio, 1997.
[43] N. Yamazoe, New approaches for improving semiconductor gas sensors, Sensors and Actuators B: Chemical, 5 (1991) 7-19.
[44] G.A.d. Wijs, P.K.d. Boer, R.A.d. Groot, G. Kresse, Anomalous behavior of the semiconducting gap in WO_3 from first-principles calculations, Physical Review B, 59 (1999) 2684.
[45] D.B. Migas, V.L. Shaposhnikov, V.N. Rodin, V.E. Borisenko, Tungsten oxides. I. Effects of oxygen vacancies and doping on electronic and optical properties of different phases of WO_3, Journal of Applied Physics, 108.
[46] M.N. Huda, Y. Yan, C.-Y. Moon, S.-H. Wei, M.M. Al-Jassim, Density-functional theory study of the effects of atomic impurity on the band edges of monoclinic WO_3, Physical Review B, 77 (2008) 195102.
[47] O.Y. Khyzhun, XPS, XES and XAS studies of the electronic structure of tungsten oxides, Journal of Alloys and Compounds, 305 (2000) 1-6.
[48] M. Hübner, C.E. Simion, A. Haensch, N. Barsan, U. Weimar, CO sensing mechanism with WO_3 based gas sensors, Sensors and Actuators B: Chemical, 151 103-106.

Authors Biographies

Mr. Mohammed Ahsan

Mr. Mohammed Ahsan has a B.Tech in Mechanical Engineering (1999) and M.S in Materials Science and Engineering (2003). He is currently a PhD candidate in Built Environment and Engineering Faculty at the Queensland University of Technology. He has an excellent research experience and publication track record in the field of materials science and engineering. He served as a Lecturer at King Fahd University of Petroleum & Minerals, Saudi Arabia from 2003-2008 and has been involved in a number of national and international projects. His research interests include nanomaterials, nanostructured thin films and nano characterization. His has over 25 publications with focus on material testing, microstructural characterization and development of thin films.

Dr. Tuquabo Tesfamichael

Dr. Tuquabo Tesfamichael received his Ph.D. in Solid State Physics in 2000 from Uppsala University, Sweden. He is serving as academic teaching and research staff at Queensland University of Technology from 2003. He has received over $2 million in research funding and awards from external competitive grants. His research has been focused on the development of metal oxide nanomaterials, thin film coatings, surface modification and thin film characterisations for solar cells and gas sensing applications. He has published over 30 refereed articles in high impact and widely read journals.

Dr. Mihail Ionescu

Dr Ionescu has a BSc (Hons) and MSc in Physics of Materials, and a PhD in Materials/Physics. He is a senior research scientist with the Ion Beam Accelerator Science Group. He has 10 years experience in superconducting materials, thin film deposition techniques and characterization of thin films. He has over 70 publications in refereed journals, over 60 conference publications, 3 book chapters and 3 patents. He is Honorary Fellow of the School of Engineering Physics, University of Wollongong. He joined ANSTO in 2004.

Professor John Bell

Professor John Bell is the Assistant Dean Research at the Queensland University of Technology, and has an excellent research funding and publication track record. He has a

wealth of experience in the synthesis of thin film electronic and optical materials, including diamond-like carbon materials and dye-sensitised titania solar cells. He also has experience in modification of materials by ion implantation and allied techniques, charge transport in photovoltaic devices, especially dye-sensitised cells, and optical phsyics. Prof. Bell has over 150 publications, the majority focussing on optical devices, and including research on photovoltaic module design for DSC cells and polymer solar cells.

Asociate Professor Nunzio Motta

Associate Professor Nunzio Motta has obtained his Laura in Physics in 1981 (Università La Sapienza – Roma) and his PhD in Physics in 1986 (Scuola Normale Superiore - Pisa). He is currently leading research at QUT in solar energy and environmental nanotechnology, developing new polymer solar cells and solar powered nanosensors. He is internationally recognized in the field of material science, with over 20 years experience in growth and characterization of nanostructures, Scanning Tunnelling Microscopy and Atomic Force Microscopy. Nunzio has obtained several visiting positions in various research institutions across Europe, published more than 110 papers in material science and surface physics and led many international research projects in the area of nanotechnology.